AIMS Mathematics, 10(1): 388−402.
DOI: 10.3934/math.2025018
Received: 09 September 2024
Revised: 13 December 2024
Accepted: 23 December 2024
Published: 08 January 2025

https://www.aimspress.com/journal/Math

Research article

Heat transfer augmentation of Jeffery–Hamel hybrid nanofluid in a stretching convergent/divergent channel through porous medium

Subhan Ullah[1], Hassan Ali Ghazwani[2], Dolat Khan[3] and Zareen A. Khan[4,*]

[1] Department of Mathematics, University of Malakand, Chakdara 18800, Pakistan
[2] Department of Mechanical Engineering, College of Engineering and Computer Sciences, Jazan University, P.O. Box 45124, Jazan, Saudi Arabia
[3] Faculty of Science, King Mongkut's University of Technology Thonburi (KMUTT), Bangkok, Thailand
[4] Department of Mathematical Sciences, College of Science, Princess Nourah bint Abdulrahman University, P.O. Box 84428, Riyadh 11671, Saudi Arabia

*** Correspondence:** Email: zakhan@pnu.edu.sa.

Abstract: The primary objective of the present study was to investigate the enhancement of heat transfer in a Jeffery–Hamel hybrid nanofluid through a porous medium, within stretching/shrinking and convergent/divergent channels. The Darcy–Forchheimer (DF) law was employed to model the flow and thermal behavior of the nanofluid. The governing system of equations was derived using appropriate transformations. Numerical computations were performed using the NDSolve method in Mathematica-11. Results are presented through numerical data and graphical representations, illustrating the effects of various physical parameters on the flow profiles. Key findings indicate that increasing the inertia coefficient and nanoparticle volume fraction accelerates the velocity of the nanofluid in both divergent and convergent channels. Furthermore, higher porosity and inertia coefficients lead to increased drag forces exerted by the channel. Jeffery–Hamel hybrid nanofluids are significantly enhanced by increasing nanoparticle volume fraction, inertia coefficient, porosity, and the presence of radiation and heat source parameters, with a notably higher rate observed in the case of an expanding channel compared to a contracting one.

Keywords: heat transfer enhancement; convergent/divergent channel; MHD; Darcy–Forchheimer space; stretching sheet
Mathematics Subject Classification: 76-10 x

Nomenclature

Symbols	Unit	Expressions	Symbols	Unit	Expressions
(r,θ)	$\frac{m}{s}$	polar coordinates	Ec		Eckert number
Fr		inertia coefficient	c_b		drag coefficient
Kp		porosity parameter	n		solid nanoparticles
k		porous permeability	Re		Reynolds number
Pr		Prandtl number	α		channel angle
k_{hnf}		thermal conductivity of hybrid nanofluid	nf	K	nanofluid
U	$\frac{m}{s}$	velocity	T_w		channel temperature
k_{nf}		thermal conductivity of nanofluid	S		stretching/shrinking rate
T	K	temperature	c_p	$\frac{kgm^2}{s.K}$	specific heat
ϕ_1,ϕ_2		hybrid nanomaterial volume friction	U_w		central line velocity
μ_{hnf}	$\frac{k\,g}{m\,s}$	dynamic viscosity of hybrid nanomaterial	ρ_{hnf}	$\frac{kg}{m^3}$	density of hybrid nanomaterial
p	$\frac{\mathrm{N}}{\mathrm{m}^2}$	pressure	S	$\frac{\mathrm{m}^2}{s}$	stretching/shrinking rate

1. Introduction

When nanometer-sized (1–100 nm) particles mix with base fluids such as water, oil, or ethylene glycol, nanofluids are formed. Nanoparticles are incredibly small particles used in a variety of applications, such as medical skin creams, environmental preservation and remediation, chemotherapy drugs, or bacterial sensors by mixing antibodies with nanotubes. Mineral particles, such as titanium oxide, are utilized in sunscreens within the cosmetics industry due to their superior long-term stability compared with conventional chemical protection. Nanomaterials are also used in athletic competitions and military applications, for instance, to create new disguise techniques by inserting mobile paint nanocrystals into the materials of soldiers' uniforms. Sensor systems also make use of nanomaterials to boost the heat capacity of a base liquid. Conductivity is the initial heat constraint when increasing heat in nanomaterials, which are made up of aluminum, oxides, carbides, iron, and carbon, among other components.

Choi [1] was the first to work with nanomaterials, and Eastman et al. [2] examined their extraordinarily high thermal conductivities. Mahanthesh et al. [3] computed the numerical solution of a magnetized nanofluid flow over a nonlinear broadened surface, and Alsabery et al. [4] described nano-liquid free conjugate convection. Nasrin et al. [5] examined the free convection of nano-liquids through a chamber and observed uncertain variations in flow patterns at various volume fraction levels. Bhatti and Rashidi [6] investigated the sound effects of thermo dispersal over a sheet in Williamson nano-liquids, and Parvin et al. [7] analyzed the complimentary convection of nano-liquids via a warped hollow space. Selimefendigil and Oztop [8] investigated nano-liquid flow through a

titled hole using a conjugated convection method. Bilal et al. [9] examined the magneto-bioconvection properties of chemically reactive nanofluids in a Darcy–Forchheimer flow. Ketchate et al. [10] analyzed magnetohydrodynamic (MHD) mixed convection flow instability of nanofluids in a porous channel, improving electronics cooling systems, heat exchangers, and car radiators.

Nanomaterials are used in medicine to provide accurate targeted heating for cancer hyperthermia therapy. Furthermore, hybrid nanofluids improve solar thermal systems' energy conversion efficiency and heat dissipation in industrial processes like metal cutting and welding. The performance of this thermal system, when exposed to a magnetic field, was investigated by Oudina et al. [11] through numerical analysis of hybrid nanofluid flow inside a porous cavity, heat transfer attributes, and entropy generation. Jamaludin et al. [12] analyzed the flow and heat transfer characteristics of hybrid nanofluids in the presence of magnetohydrodynamics and heat sources. Other models have explored nanofluid applications [13−17].

Porous media are hard mixtures with connected voids (pores) that transfer liquids under pressure gradients. This allows improved combustion efficiency and minimizes pollution due to the homogeneous radioactive heat flow. Porous media has different industrial applications, including residential heaters, gas turbines, automobile heaters, fuel cells, and energy management. Verma et al. [18] showed that the suction effect in nanofluids with porous media enhances heat transfer rates and the skin friction coefficient. Kapen et al. [19] found that suction in porous media reduces drag and maintains steady flow. The intricate flow patterns produced by the interaction of suction and porous media may aid in cooling effectiveness and heat transfer augmentation. Through numerical analysis, researchers investigated the steady boundary layer free convection flow over a horizontal flat plate inserted into a porous medium containing two salts and a water-based nanofluid. Khan et al. [20] investigated the dual nature of the solution for heat transfer and fluid flow across a stretching/shrinking sheet in porous media, and Uddin et al. [21] evaluated the bio-nano-convection flow in a porous media with blowing effects.

Jeffery–Hamel flow refers to a two-dimensional, incompressible fluid flow between non-parallel, divergent/convergent (CD) channels that are inclined at a fixed angle and determined by a line inflow or outflow located at the end. This flow configuration can also involve stretching/shrinking of the channels, adding complexity to fluid dynamics. Jeffery–Hamel flow is essential in aerospace engineering for estimating fluid behavior in a variety of channel geometries, aiding the design of effective rocket nozzles and supersonic wind tunnels. It also has applications in the non-Newtonian fluid optimization of reactors and mixers in chemical engineering, enhancing process efficiency, and in the study of blood flow in artery narrowing for biomedical applications to improve the design of medical devices (e.g., stents). In addition, this flow model is utilized in heat transfer and microfluidics systems to maximize cooling and fluid distribution. George Barker Jeffery [22] in 1915 and Georg Hamel [23] in 1917 worked in the Jeffery–Hamel flow model. Ara et al. [24] explored heat transfer in Jeffery–Hamel flow under Lorentz forces, and Turkyilmazoglu et al. [25] extended the conventional Jeffery–Hamel flow to stretchable convergent/divergent channels. Hafeez et al. [26] examined heat transfer characteristics of Jeffery–Hamel flow of hybrid nanofluids in divergent and convergent channels. The wavelet technique was employed by Kumbinarasaiah and Raghunatha [27] to examine the numerical solution of the Jeffery–Hamel flow. Biswal et al. [28] characterized the flexibility of nanofluids using flexible inclined plates. Qadeer et al. [29] examined the convergent/divergent aspects of nanofluid flow using irreversibility analysis. Abdelouahab et al. [30] investigated the combined effects of rotation and thermal radiation on heat and mass transfer in magnetohydrodynamic flow within converging/diverging walls. Mohamed et al. [31] investigated heat transfer in electro-magnetohydrodynamic ternary hybrid nanofluid flow through

extending/narrowing walls with stretching/shrinking channels.

Based on this literature review, this study aims to enhance heat transfer in Jeffery–Hamel hybrid nanofluids through porous media in stretching/shrinking and convergent/divergent channels. The Darcy–Forchheimer (DF) law is employed to model the flow and thermal properties of the nanofluid, with the governing equations derived using appropriate transformations. Numerical computations are conducted using the NDSolve method in Mathematica-11, and the results are analyzed through numerical data and graphical representations. Key findings reveal that increasing the nanoparticle volume fraction and inertia coefficient significantly accelerates nanofluid velocity in both divergent and convergent channels. Additionally, higher porosity and inertia coefficients enhance drag forces, and the presence of radiation and heat source parameters further boost the heat transfer rate. A notable higher enhancement is observed in expanding channels compared to contracting ones. This study introduces novel insights into the interplay of hybrid nanofluids and porous media in varying channel geometries, presenting valuable contributions for optimizing heat transfer in engineering applications.

2. Materials and methods

Let us consider the non-Newtonian behavior of incompressible Jeffrey fluids in the presence of two anisotropic, divergent/convergent, and stretching/shrinking channels. In this scenario, the polar coordinate system is applied since there is an angle of two between two walls. The velocity field for Jeffery fluid is $V=[u(r,\theta),0,0]$. The channel walls contract and expand with radial velocity $u=u_w=\frac{s}{r}$, as show in Figure 1. Liquid velocity only occurs at a radial path. The channel stretches when $c>0$; otherwise, it shrinks.

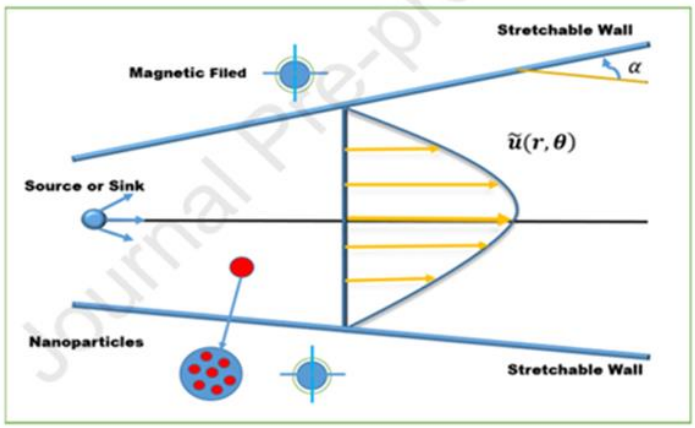

Figure 1. Geometrical visualization of the model.

2.1. Continuity equation

$$\frac{1}{r}\frac{\partial}{\partial r}(ru)=0, \tag{1}$$

2.2. Velocity equation

$$u\frac{\partial u}{\partial r}=-\frac{1}{\rho_{hnf}}\frac{\partial p}{\partial r}+\frac{\mu_{hnf}}{\rho_{hnf}}\left(\frac{1}{r}\frac{\partial u}{\partial r}-\frac{u}{r}+\frac{\partial^2 u_r}{\partial r^2}+\frac{1}{r^2}\frac{\partial^2 u}{\partial\theta^2}\right)-\frac{\nu_f}{\rho_{hnf}}\frac{u}{k}-Fu^2, \tag{2}$$

$$\frac{2}{r^2}\frac{\mu_{hnf}}{\rho_{hnf}}\frac{\partial u}{\partial\theta}-\frac{1}{r\rho_{hnf}}\frac{\partial p}{\partial\theta}=0. \tag{3}$$

2.3. Energy equation

$$u\frac{\partial T}{\partial r}=\frac{k_{hnf}}{(\rho c_p)_{hnf}}\left(\frac{1}{r}\frac{\partial T}{\partial r}+\frac{\partial^2 T}{\partial r^2}+\frac{1}{r^2}\frac{\partial^2 T}{\partial\theta^2}\right)+\mu_{hnf}\left(\left(\frac{\partial u}{\partial r}\right)^2+\frac{1}{r}\left(\frac{\partial u}{\partial\Theta}\right)^2\right). \tag{4}$$

Equations (1)–(3) are the main equations of continuity, momentum, and energy [32].

2.4. Boundary conditions

The boundary conditions are as follows [33]:

$$\left.\begin{aligned} u=\frac{U}{r},\ \frac{\partial u}{\partial\theta}=0,\ \frac{\partial T}{\partial\theta}=0\ \ at\ \ \theta=0, u_r=U_w=\frac{s}{r},\ T=\frac{T_w}{r^2}\ at\ \ \theta=\alpha. \end{aligned}\right\} \tag{5}$$

Here, p designates pressure, U represents the center line velocity, and U_w depicts the velocity of the channel wall. Furthermore, k is the porous media permeability, and F represents the irregular inertia parameter. T_w is the wall temperature. Additionally, ρ_{hnf}, μ_{hnf} represent the thermal conductivity and heat capacity of the hybrid nanomaterial, respectively.

The thermophysical properties of hybrid nanomaterials are described as follows [34]:

$$\left.\begin{aligned} &\frac{\mu_{hnf}}{\mu_f}=\frac{1}{(1-\phi_1)^{2.5}(1-\phi_2)^{2.5}},\\ &\frac{\rho_{hnf}}{\rho_f}=(1-\phi_2)\left((1-\phi_1)+\phi_1\left(\frac{\rho_{s1}}{\rho_f}\right)+\phi_2\left(\frac{\rho_{s2}}{\rho_f}\right)\right),\\ &\frac{(\rho c_p)_{hnf}}{(\rho c_p)_f}=(1-\phi_2)\left((1-\phi_1)+\phi_1\left(\frac{(\rho c_p)_{s1}}{(\rho c_f)_f}\right)\right)+\phi_2\left(\frac{(\rho c_p)_{s2}}{(\rho c_p)_f}\right),\\ &\frac{k_{hnf}}{k_{bf}}=\frac{2k_{bf}+k_{s2}-2\phi_2(k_f-k_{s2})}{2k_{bf}+k_{s2}+\phi_2(k_f-k_{s2})}. \end{aligned}\right\}$$

Where

$$\frac{k_{bf}}{k_f}=\frac{k_{s1}+2k_f-2\phi_1(k_f-k_{s1})}{k_{s1}+k_f+\phi_1(k_f-k_{s1})}.$$

In the above equations, n represents solid nanoparticles of the base fluid, $\left(\rho c_p\right)_f$ designates the heat capacity, and $\left(\rho c_p\right)_{s1}, \left(\rho c_p\right)_{s2}$ are the heat capacitance of hybrid nanomaterials. Furthermore, ϕ_1, ϕ_2 describe the volume friction of the hybrid nanomaterial. ρ_f represents the density of the base fluid, and ρ_{s1}, ρ_{s2} designate the densities of the hybrid nanoparticles. Similarly, k_f depicts the thermal conductivity of the base fluid, and k_{s1}, k_{s2} describe the thermal conductivities of hybrid nanoparticles.

$$F(\theta) = r\,u(r,\theta). \tag{6}$$

The similarity variable can be written as:

$$f(\eta) = \frac{F(\theta)}{U},\ \eta = \frac{\theta}{\alpha},\ \Phi = r^2\frac{T}{T_w}. \tag{7}$$

$$\left.\begin{aligned} &f''' + 2\alpha\,\mathrm{Re}\left(1-\phi_1\right)^{2.5}\left(1-\phi_2\right)^{2.5}\left(\left(1-\phi_2\right)\left(\left(1-\phi_1\right)+\phi_1\left(\frac{\rho_{s_1}}{\rho_f}\right)+\phi_2\left(\frac{\rho_{s_2}}{\rho_f}\right)\right)\right)ff' + \\ &\left(4-k_p\left(\left(1-\phi_1\right)^{2.5}\left(1-\phi_2\right)^{2.5}\right)\left(1-\phi_2\right)\left(1-\phi_1\right)+\phi_1\left(\frac{\rho_{s_1}}{\rho_f}\right)+\phi_2\left(\frac{\rho_{s_2}}{\rho_f}\right)\right)\alpha^2 f' + \\ &2\alpha^2 Fr\left(1-\phi_1\right)^{2.5}\left(1-\phi_2\right)^{2.5}\left(\left(1-\phi_2\right)\left(1-\phi_1\right)+\phi_1\left(\frac{\rho_{s_1}}{\rho_f}\right)+\phi_2\left(\frac{\rho_{s_2}}{\rho_f}\right)\right)f'^2 = 0, \end{aligned}\right\} \tag{8}$$

$$\left.\begin{aligned} &\frac{k_{hnf}}{k_f}\left(\Phi'' + 4\alpha^2\Phi\right) + 2\,\mathrm{Pr}\left(\left(1-\phi_2\right)\left(1-\phi_1\right)+\phi_1\frac{\left(\rho c_p\right)_{s1}}{\left(\rho c_p\right)_f}\right)+\phi_2\left(\frac{\left(\rho c_p\right)_{s2}}{\left(\rho c_p\right)_f}\right)\alpha^2\Phi f + \\ &\frac{\mathrm{Pr}\,Ec}{\mathrm{Re}\left(1-\phi_1\right)^{2.5}\left(1-\phi_2\right)^{2.5}}\left(\left(1-\phi_2\right)\left(\left(1-\phi_1\right)+\phi_1\frac{\left(\rho c_p\right)_{s1}}{\left(\rho c_p\right)_f}\right)+\phi_2\left(\frac{\left(\rho c_p\right)_{s2}}{\left(\rho c_p\right)_f}\right)\right)\left(4\alpha^2 f^2 + f'^2\right) = 0. \end{aligned}\right\} \tag{9}$$

Applying the transformation to the initial and boundary conditions,

$$f(0) = 0,\ \ f'(0) = 0,\ \ \Phi'(0) = 0,\ \ f(1) = S,\ \ \Phi(1) = 1. \tag{10}$$

Here, $K_p = \frac{v_f}{kU}$ is the porosity parameter, $Ec = \frac{U^2\alpha}{K_{hnf}}$ represents the Eckert number, $Fr = \frac{cb}{\sqrt{k}}$ is the Darcy-Forchheimer law, $\mathrm{Pr} = \frac{\left(\rho c_p\right)_f U}{k_{hnf}}$ is the Prandtl number, and $S = \frac{s}{U}$ is the stretching parameter. When $(\alpha < 0)$, the channel is convergent; otherwise, it is divergent.

2.5. Physical quantities

The physical quantities are as follows:

$$\mathrm{Re}\,C_f = \frac{f'(1)}{(1-\phi_1)^{2.5}(1-\phi_2)^{2.5}\left((1-\phi_2)\left((1-\phi_1)+\phi_1\left(\frac{\rho_{s1}}{\rho_f}\right)\right)+\phi_2\left(\frac{\rho_{s2}}{\rho_f}\right)\right)}, \tag{11}$$

$$\alpha Nu = \frac{k_{hnf}}{k_f}\Phi'(1). \tag{12}$$

3. Numerical techniques

The main system of Eqs (8) and (9) with associated boundary conditions (10) are solved numerically using the NDSolve method with Mathematica-11 software. The main system of ordinary differential equations (ODEs) covers various expressions represented by $(H_1, H_2, H_3.....H_n)$ with the independent variable ξ and the dependent variable n with $(K_1, K_2, K_3, ...K_n)$. The reputable partial differential equation (PDE) system also presents boundary conditions.

NDSolve [{$(H_1, H_2, H_3.....H_n)$, BCs}, $(K_1, K_2, K_3, ...K_n)$, {ξ, ξmin, ξmax}].

The suggested mathematical model is shown in Figure 2.

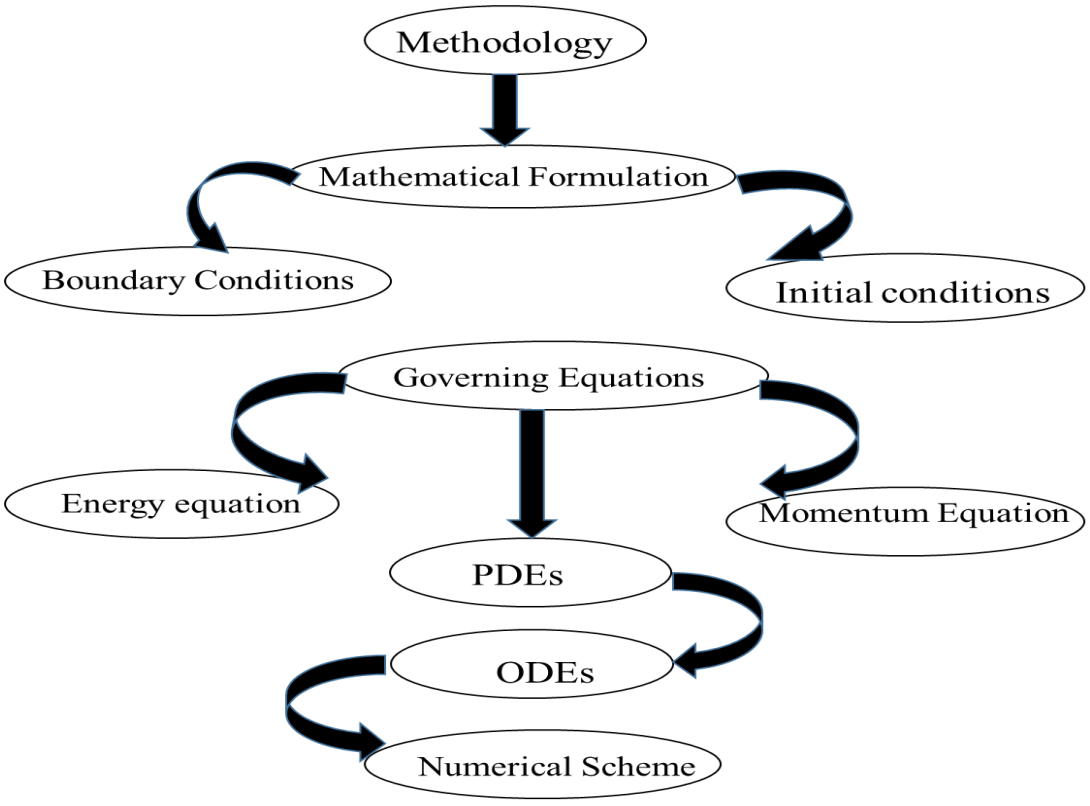

Figure 2. Flowchart of the mathematical model.

4. Discussion outcomes

In this section, the behavior of the physical parameters porosity, Reynolds number, inertia, and

volume friction ($Kp, \mathrm{Re}, Fr, \phi_1, \phi_2$) and the Eckert number (Ec) is investigated against the velocity $f(\eta)$ and temperature $\Theta(\eta)$ profiles. Results show ranging values as follows: $Kp = (50-200), \mathrm{Re} = (05-20), Ec = (0.2-0.8), \phi_1 = (0.01-0.04), \phi_2 = Fr = (10-40)$. Significant physical quantities such as the Nusselt number N_u and skin friction C_f are analyzed based on different variables such as Kp, Fr, Re , and Ec in Tables 1 and 2.

4.1. Velocity profile

In this section, $Kp, \mathrm{Re}, Fr, \phi_1, \phi_2$ are examined against velocity $f(\eta)$ for both convergent and divergent $(\alpha < 0, \alpha > 0)$ channels. Figure 3 depicts the porosity parameter Kp , ranging from 50 to 200 against $f(\eta)$ for converging/diverging $(\alpha < 0, \alpha > 0)$ channels. This shows that higher values of Kp result in enhanced velocity in both extending and narrowing $(\alpha < 0, \alpha > 0)$ channels. Where the thermophysical properties of base fluids and nanoparticles is represented in Table 1. Figure 4 shows that the velocity profile $f(\eta)$ increases in convergent cases when the Reynolds number increases; on the other hand, there is an opposite trend in the divergent case. By increasing the Reynolds number Re, $f(\eta)$ decreases as a result of reverse motion generating new drag forces in the flow, which increases resistance to velocity away from the channel wall. When the inertia parameter increases, $f(\eta)$ is enhanced in both extending and narrowing channels (Figure 5). Figures 6 and 7 show the behavior of volume friction parameters ϕ_1 and ϕ_2 for extending and narrowing walls, showing a similar influence against velocity variations $f(\eta)$ for both divergent/convergent channels.

Table 1. Thermophysical properties of base fluids and nanoparticles [35].

Physical properties	$c_p\left(\frac{J}{kgK}\right)$	K	$\rho\left(\frac{kg}{m^3}\right)$	$\frac{\beta \times 10^{-5}}{K}$	Pr
Kerosene oil	2090	0.145	783	99	21
Gold	717	5000	1800	28.4	
Water	4179	0.613	997.1	21	6.2
Ag	235	429	10,500	1.89	

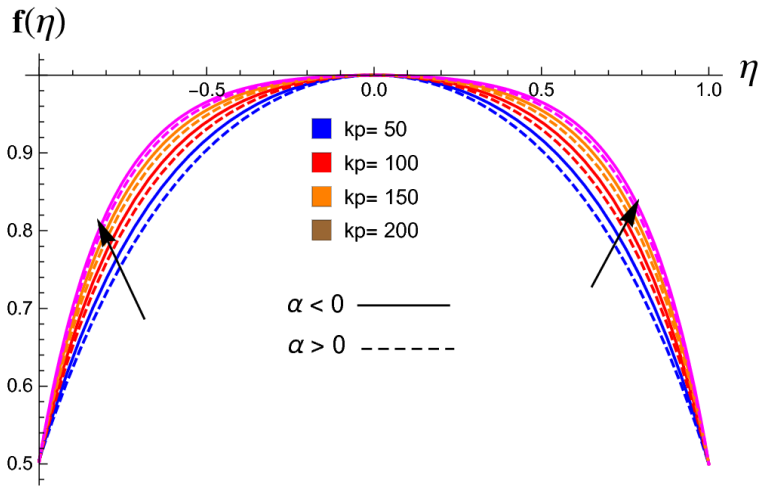

Figure 3. Behavior of velocity ($f(\eta)$) against the porosity parameter (Kp).

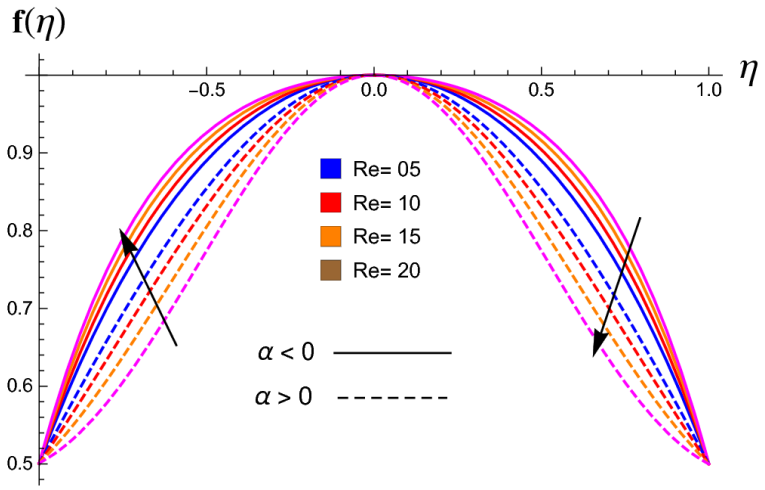

Figure 4. Behavior of velocity ($f(\eta)$) against the Reynolds number (Re).

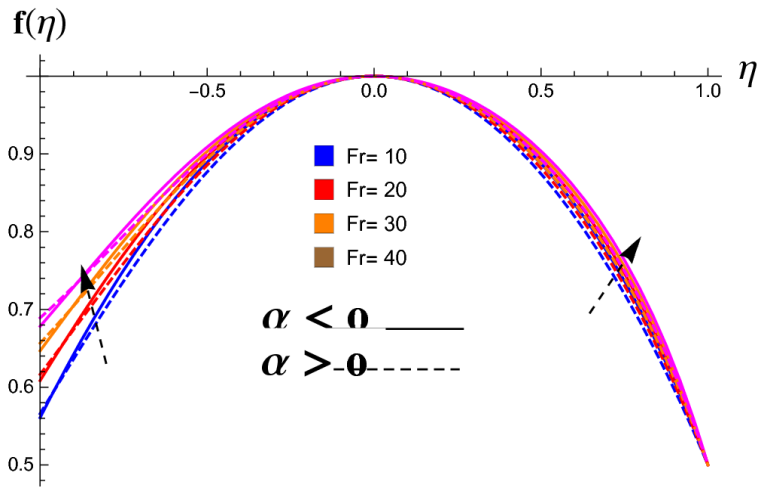

Figure 5. Behavior of velocity ($f(\eta)$) against the inertia parameter (Fr).

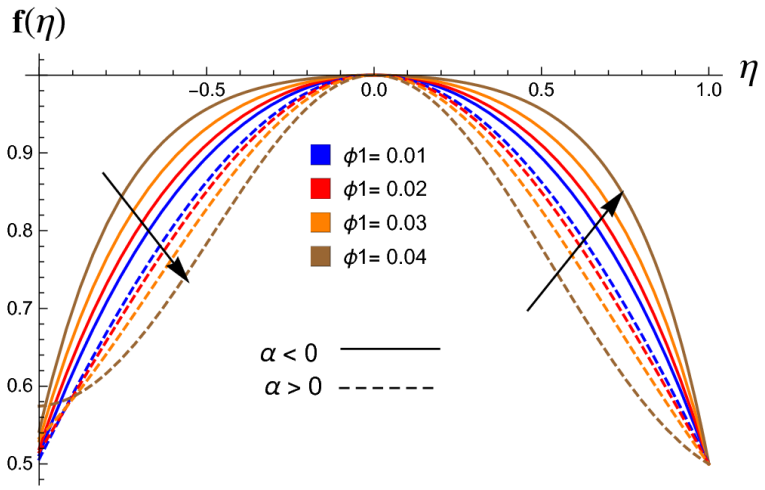

Figure 6. Behavior of velocity ($f(\eta)$) against volume friction (ϕ_1).

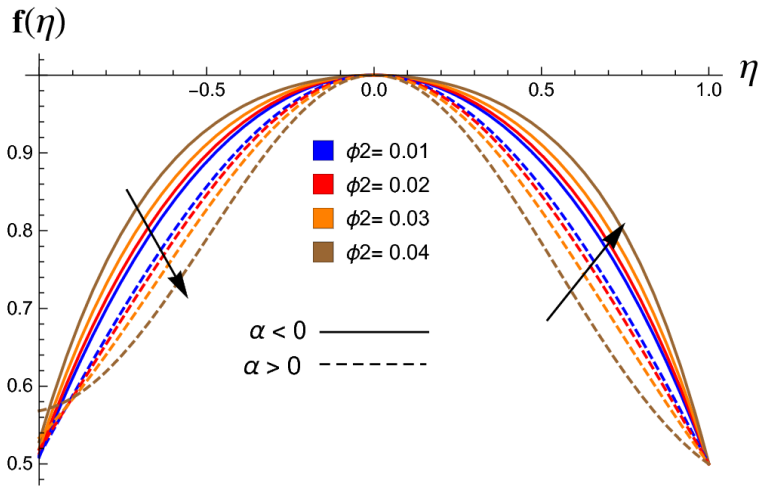

Figure 7. Behavior of velocity ($f(\eta)$) against volume friction (ϕ_2).

4.2. Temperature profile

The influence of Eckert number (Ec) and Reynolds number (Re) on the temperature ($\Theta(\eta)$) profile for divergent and convergent channels is illustrated in Figures 8 and 9, respectively. Ec ranges from 0.2 to 0.8; the higher the Eckert number, the higher the temperature for extending and narrowing $(\alpha < 0, \alpha > 0)$ walls. Physically, the nanoparticle temperature increases with higher values of Ec in both convergent and divergent walls. Viscosity and dissipative energy are physically enhanced by higher Eckert number estimations.

A higher Reynolds number results in higher temperatures in the convergent case, while the opposite is true in the divergent case. This distinction is critical; in a convergent channel, the temperature rises with increasing Reynolds number due to enhanced fluid compression and heat accumulation. In contrast, in a divergent channel, the temperature decreases as the flow expands, leading to heat dissipation and reduced thermal energy concentration. These opposing effects emphasize the differential thermal dynamics in varying channel geometries. This notion is essential

for understanding and optimizing heat transfer in diverse engineering applications.

Table 2 analyzes the Nusselt number for both extending/narrowing $(\alpha < 0, \alpha > 0)$ channels; the convergent channel has higher capability to improve the heat transfer rate than the divergent channel.

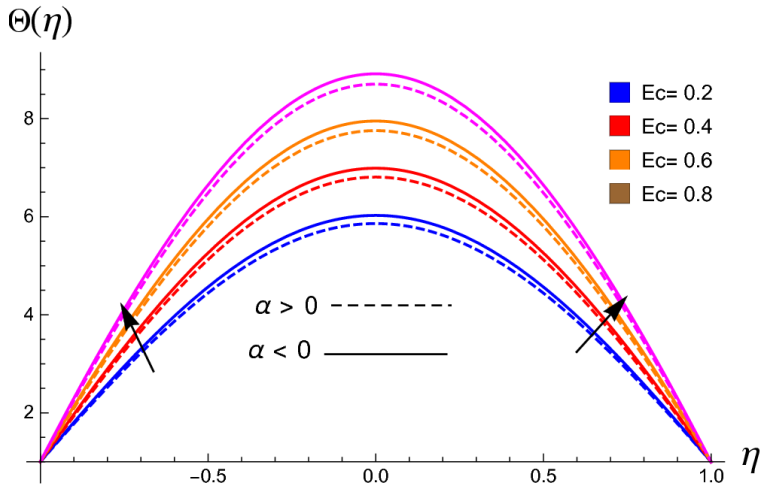

Figure 8. Behavior of temperature ($\Theta(\eta)$) against the Eckert number (Ec).

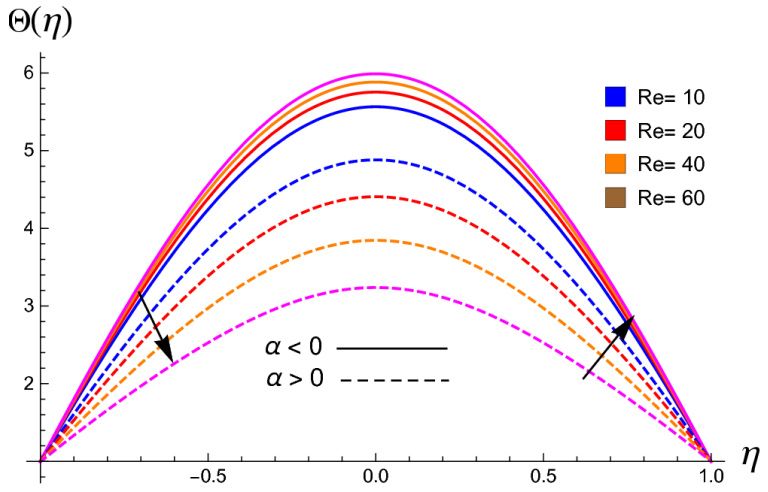

Figure 9. Behavior of temperature ($\Theta(\eta)$) against the Reynolds number (Re).

Table 2. Analysis of the Nusselt number in divergent/convergent channels.

	Divergent channel ($\alpha > 0$)		Convergent channel ($\alpha < 0$)	
ϕ	Nu	%age	Nu	%age
0.00	1.706		1.053	
0.01	1.906	11.72333	1.253	18.99335
0.02	1.936	13.48183	1.283	21.84236
0.03	1.966	15.24033	1.313	24.69136
0.04	1.996	16.99883	1.343	27.54036

5. Conclusions

This study investigates the enhancement of heat transfer in Jeffery–Hamel hybrid nanofluids in the presence of porous media within stretching/shrinking and convergent/divergent $(\alpha < 0, \alpha > 0)$ channels. Utilizing the Darcy–Forchheimer (DF) law, the flow and thermal behaviors of the nanofluid are modeled, and the governing equations are derived through suitable transformations. Numerical solutions are obtained using the NDSolve method in Mathematica-11, with results presented in both numerical and graphical formats. The findings reveal that increasing the inertia coefficient and nanoparticle volume fraction accelerates fluid velocity in both channel types, while drag forces are amplified by higher porosity and inertia coefficients. Notably, the heat transfer rate is improved by radiation and heat source parameters; this is more significant in expanding channels. These insights provide a deeper understanding of hybrid nanofluids' dynamics and their potential for engineering applications. The most important results are listed below:

- Velocity increased for both convergent/divergent channels due to larger values of Kp.
- Velocity was enhanced in the convergent case and reduced in the divergent case for several Reynolds number.
- Hybrid nanofluids make a more significant contribution to the velocity field.
- Temperature is enhanced for greater values of the Eckert number in both convergent/divergent channels.
- Greater values of Reynolds number lead to increases in temperature in convergent channels and decreased temperature in divergent channels.
- This phenomenon has important applications for environmental science and medical engineering.
- The current research work may be applied to improve the efficiency and structure of heat exchangers by modified designs. It can also be applied to solar energy systems.

Future directions: Future researchers can build on this work by exploring alternative nanofluid compositions, including eco-friendly or biodegradable materials, to enhance performance while maintaining environmental sustainability. Extending the study to three-dimensional flows or more complex geometries could provide greater applicability to real-world scenarios. Experimental validation of numerical findings would also be valuable in bridging theoretical models with practical outcomes. Investigating transient or turbulent flow conditions and incorporating nonlinear effects such as temperature-dependent properties or nanoparticle interactions could lead to more comprehensive models.

Author contributions

Subhan Ullah and Hassan Ali Ghazwani: Conceptualization, writing - original draft; Dolat Khan: Investigation, supervision; Subhan Ullah: Software; Subhan Ullah and Zareen A. Khan: Writing - review editing; Dolat Khan and Zareen A. Khan: Visualization.

Use of Generative-AI tools declaration

The authors declare they have not used Artificial Intelligence (AI) tools in the creation of this article.

Acknowledgments

Princess Nourah bint Abdulrahman University Researchers Supporting Project number (PNURSP2024R8). Princess Nourah bint Abdulrahman University, Riyadh, Saudi Arabia.

Conflict of interest

All authors declare no conflicts of interest in this paper.

References

1. S. U. S. Choi, D. A. Singer, H. P. Wang, Developments and applications of non-Newtonian flows, *Asme Fed*, **66** (1995**)**, 99−105.
2. J. A. Eastman, U. S. Choi, S. Li, L. J. Thompson, S. Lee, *Enhanced thermal conductivity through the development of nanofluids*, In: MRS Online Proceedings Library (OPL), Cambridge University Press, **457** (1996). https://doi.org/10.1557/PROC-457-3
3. B. Mahanthesh, B. J. Gireesha, R. R. Gorla, F. M. Abbasi, S. A. Shehzad, Numerical solutions for magnetohydrodynamic flow of nanofluid over a bidirectional non-linear stretching surface with prescribed surface heat flux boundary, *J. Magn. Magn. Mater.*, **417** (2016), 189−196. https://doi.org/10.1016/j.jmmm.2016.05.051
4. A. I. Alsabery, A. J. Chamkha, H. Saleh, I. Hashim, Heatline visualization of conjugate natural convection in a square cavity filled with nanofluid with sinusoidal temperature variations on both horizontal walls, *Int. J. Heat Mass Tran.*, **100** (2016), 835−850. https://doi.org/10.1016/j.ijheatmasstransfer.2016.05.031
5. R. Nasrin, M. A. Alim, A. J. Chamkha, Buoyancy-driven heat transfer of water-Al_2O_3 nanofluid in a closed chamber: Effects of solid volume fraction, Prandtl number and aspect ratio, *Int. J. Heat Mass Tran.*, **55** (2012), 7355−7365. https://doi.org/10.1016/j.ijheatmasstransfer.2012.08.011
6. M. M. Bhatti, M. M. Rashidi, Effects of thermo-diffusion and thermal radiation on Williamson nanofluid over a porous shrinking/stretching sheet, *J. Mol. Liq.*, **221** (2016), 567−573. https://doi.org/10.1016/j.molliq.2016.05.049
7. S. Parvin, R. Nasrin, M. A. Alim, N. F. Hossain, A. J. Chamkha, Thermal conductivity variation on natural convection flow of water-alumina nanofluid in an annulus, *Int. J. Heat Mass Tran.*, **55** (2012), 5268−5274. https://doi.org/10.1016/j.ijheatmasstransfer.2012.05.035
8. F. Selimefendigil, H. F. Öztop, Conjugate natural convection in a cavity with a conductive partition and filled with different nanofluids on different sides of the partition, *J. Mol. Liq.*, **216** (2016), 67−77. https://doi.org/10.1016/j.molliq.2015.12.102
9. S. Bilal, K. Pan, Z. Hussain, B. Kada, A. A. Pasha, W. A. Khan, Darcy-Forchheimer chemically reactive bidirectional flow of nanofluid with magneto-bioconvection and Cattaneo-Christov properties, *Tribol. Int.*, **193** (2024), 109313. https://doi.org/10.1016/j.triboint.2024.109313
10. C. G. N. Ketchate, P. T. Kapen, D. Fokwa, G. Tchuen, Instability of MHD mixed convection flow of nanofluid in porous channel with thermal radiation, chemical reaction, Dufour and Soret effects, *Chinese J. Phys.*, **87** (2024), 728−750. https://doi.org/10.1016/j.cjph.2023.10.019
11. F. Mebarek-Oudina, I. Chabani, H. Vaidya, A. A. I. Ismail, Hybrid-nanofluid magneto-convective flow and porous media contribution to entropy generation, *Int. J. Numer. Method. H.*, **34** (2024), 809−836. https://doi.org/10.1108/HFF-06-2023-0326

12. A. Jamaludin, N. A. A. M. Nasir, R. Nazar, I. Pop, MHD opposing flow of Cu-TiO_2 hybrid nanofluid under an exponentially stretching/shrinking surface embedded in porous media with heat source and slip impacts, *Results Eng.*, **17** (2023), 101005. https://doi.org/10.1016/j.rineng.2023.101005
13. D. Khan, K. K. Asogwa, N. Akkurt, P. Kumam, W. Watthayu, K. Sitthithakerngkiet, Development of generalized Fourier and Fick's law of electro-osmotic MHD flow of sodium alginate based Casson nanofluid through inclined microchannel: Exact solution and entropy generation, *Sci. Rep.*, **12** (2022), 18646. https://doi.org/10.1038/s41598-022-21854-5
14. A. Khan, F. ul Karim, I. Khan, T. A. Alkanhal, F. Ali, D. Khan, et al., Entropy generation in MHD conjugate flow with wall shear stress over an infinite plate: Exact analysis, *Entropy*, **21** (2019), 359. https://doi.org/10.3390/e21040359
15. D. Khan, P. Kumam, W. Watthayu, I. Khan, Heat transfer enhancement and entropy generation of two working fluids of MHD flow with titanium alloy nanoparticle in Darcy medium, *J. Therm. Anal. Calorim.*, **147** (2022), 10815−10826. https://doi.org/10.1007/s10973-022-11284-w
16. H. M. Mobarak, E. M. Abo-Eldahab, R. Adel, M. Abdelhakem, MHD 3D nanofluid flow over nonlinearly stretching/shrinking sheet with nonlinear thermal radiation: Novel approximation via Chebyshev polynomials' derivative pseudo-Galerkin method, *Alex. Eng. J.*, **102** (2024), 119−131. https://doi.org/10.1016/j.aej.2024.05.069
17. D. Khan, M. A. Hussien, A. M. A. Elsiddieg, S. A. Lone, A. M. Hassan, Exploration of generalized two-phase free convection magnetohydrodynamic flow of dusty tetra-hybrid Casson nanofluid between parallel microplates, *Nanotechnol. Rev.*, **12** (2023), 20230102. https://doi.org/10.1515/ntrev-2023-0102
18. A. K. Verma, A. K. Gautam, K. Bhattacharyya, R. P. Sharma, Existence of boundary layer nanofluid flow through a divergent channel in porous medium with mass suction/injection, *Sādhanā*, **46** (2021), 98. https://doi.org/10.1007/s12046-021-01588-2
19. P. T. Kapen, C. G. N. Ketchate, D. Fokwa, G. Tchuen, Linear stability analysis of (Cu-Al_2O_3)/water hybrid nanofluid flow in porous media in presence of hydromagnetic, small suction and injection effects, *Alex. Eng. J.*, **60** (2021), 1525−1536. https://doi.org/10.1016/j.aej.2020.11.007
20. Z. H. Khan, W. A. Khan, I. Pop, Triple diffusive free convection along a horizontal plate in porous media saturated by a nanofluid with convective boundary condition, *Int. J. Heat Mass Tran.*, **66** (2013), 603−612. https://doi.org/10.1016/j.ijheatmasstransfer.2013.07.074
21. M. J. Uddin, N. A. Amirsom, O. A. Bég, A. I. Ismail, Computation of bio-nano-convection power law slip flow from a needle with blowing effects in a porous medium, *Wave. Random Complex*, 2022, 1−21. https://doi.org/10.1080/17455030.2022.2048919
22. G. B. Jeffery, *The two-dimensional steady motion of a viscous fluid*, The London, Edinburgh, and Dublin Philosophical Magazine and Journal of Science, **29** (1915), 455−465. https://doi.org/10.1080/14786440408635327
23. G. Hamel, Spiralformige bewegungen zaher flussigkeiten, *Jahresbericht Der Deutschen Mathematiker Vereinigung*, **25** (1917), 34−60.
24. A. Ara, N. A. Khan, F. Sultan, S. Ullah, Numerical simulation of Jeffery-Hamel flow of Bingham plastic fluid and heat transfer in the presence of magnetic field, *Appl. Comput. Math.*, **18** (2019), 135−148.
25. M. Turkyilmazoglu, Extending the traditional Jeffery-Hamel flow to stretchable convergent/divergent channels, *Comput. Fluids*, **100** (2014), 196−203. https://doi.org/10.1016/j.compfluid.2014.05.016

26. M. Hafeez, Hashim, M. Khan, Jeffery-Hamel flow of hybrid nanofluids in convergent and divergent channels with heat transfer characteristics, *Appl. Nanosci.*, **10** (2020), 5459−5468. https://doi.org/10.1007/s13204-020-01427-6
27. S. Kumbinarasaiah, K. R. Raghunatha, Numerical solution of the Jeffery-Hamel flow through the wavelet technique, *Heat Transfer*, **51** (2022), 1568−1584. https://doi.org/10.1002/htj.22364
28. U. Biswal, S. Chakraverty, B. K. Ojha, A. K. Hussein, Numerical investigation on nanofluid flow between two inclined stretchable walls by Optimal Homotopy Analysis Method, *J. Comput. Sci.*, **63** (2022), 101759. https://doi.org/10.1016/j.jocs.2022.101759
29. M. Qadeer, U. Khan, S. Ahmad, B. Ullah, M. Mousa, I. Khan, Irreversibility analysis for flow of nanofluids with aggregation in converging and diverging channel, *Sci. Rep.*, **12** (2022), 10214. https://doi.org/10.1038/s41598-022-14529-8
30. A. Bouchireb, M. Kezzar, A. Dib, M. R. Sari, M. R. Eid, E. M. Elsaid, Combined effects of rotating and thermal radiation on heat and mass transfer of MHD flow in converging and diverging channels, *Int. J. Model. Simul.*, 2024, 1−20. https://doi.org/10.1080/02286203.2024.2343997
31. M. Kezzar, G. Sowmya, N. Talbi, H. Berrehal, M. R. Sari, I. Tabet, et al., Heat transfer scrutiny in EMHD ternary hybrid nanofluid flow between convergent/divergent channels with stretchable walls, *Int. J. Model. Simul.*, 2024, 1−16. https://doi.org/10.1080/02286203.2024.2338580
32. G. K. Ramesh, S. A. Shehzad, I. Tlili, Hybrid nanomaterial flow and heat transport in a stretchable convergent/divergent channel: A Darcy-Forchheimer model, *Appl. Math. Mech.*, **41** (2020), 699−710. https://doi.org/10.1007/s10483-020-2605-7
33. A. S. Alnahdi, S. Nasir, T. Gul, Ternary Casson hybrid nanofluids in convergent/divergent channel for the application of medication, *Therm. Sci.*, **27** (2023), 67−76. https://doi.org/10.2298/TSCI23S1067A
34. M. Kezzar, A. Nehal, P. Ragupathi, S. Saranya, U. Khan, M. R. Sari, et al., Implication of electromagnetohydrodynamic flow of a non-Newtonian hybrid nanofluid in a converging and diverging channel with velocity slip effects: A comparative investigation using numerical and ADM approaches, *ZAMM*, **104** (2024), e202300872. https://doi.org/10.1002/zamm.202300872
35. D. Khan, P. Kumam, W. Watthayu, Multi-generalized slip and ramped wall temperature effect on MHD Casson fluid: Second law analysis, *J. Therm. Anal. Calorim.*, **147** (2022), 13597−13609. https://doi.org/10.1007/s10973-022-11482-6